Geophysical Research Letters

RESEARCH LETTER
10.1029/2022GL102710

Conditions for Inception of Relativistic Runaway Discharges in Air

Victor P. Pasko[1], Sebastien Celestin[2], Anne Bourdon[3], Reza Janalizadeh[1], and Jaroslav Jansky[4]

[1]School of Electrical Engineering and Computer Science, Penn State University, University Park, PA, USA, [2]Laboratory of Physics and Chemistry of the Environment and Space (LPC2E), CNRS, University of Orleans, Orleans, France, [3]Plasma Physics Laboratory (LPP), Ecole Polytechnique, Palaiseau, France, [4]Department of Mathematics and Physics, University of Defense, Brno, Czechia

Key Points:

- The onset of terrestrial gamma ray flashes is linked to the spatial extent of the lightning leader streamer zone
- The photoelectric absorption is the dominant feedback factor defining inception of relativistic runaway discharges in air
- The photoelectric absorption generated runaway electrons from the cathode facilitate X-rays from laboratory sparks

Supporting Information:

Supporting Information may be found in the online version of this article.

Correspondence to:

V. P. Pasko,
vpasko@psu.edu

Citation:

Pasko, V. P., Celestin, S., Bourdon, A., Janalizadeh, R., & Jansky, J. (2023). Conditions for inception of relativistic runaway discharges in air. *Geophysical Research Letters*, *50*, e2022GL102710. https://doi.org/10.1029/2022GL102710

Received 29 DEC 2022
Accepted 23 FEB 2023

Abstract Terrestrial gamma-ray flashes are linked to growth of long bidirectional lightning leader system consisting of positive and stepping negative leaders. The spatial extent of streamer zones of a typical lightning leader with tip potential exceeding several tens of megavolts is on the order of 10–100 m. The photoelectric absorption of bremsstrahlung radiation generated by avalanching relativistic runaway electrons occurs efficiently on the same spatial scales. The intense multiplication of these electrons is triggered when the size of the negative leader streamer zone crosses a threshold of approximately 100 m (for sea-level air pressure conditions) allowing self-replication of these avalanches due to the upstream relativistic electron seeds generated by the photoelectric absorption. The model results also highlight importance of electrode effects in interpretation of X-ray emissions from centimeter to meter long laboratory discharges, in particular, a similar feedback effect produced by generation of runaway electrons from the cathode material.

Plain Language Summary We propose a physical mechanism that explains spectacular naturally occurring bursts of X-rays that are observed in association with lightning activity in the Earth's atmosphere. These events are commonly referred to as terrestrial gamma ray flashes (TGFs). The mechanism is based on a feedback process allowing amplification of relativistic electron avalanches when X-rays emitted by these electrons travel backwards with respect to the electron motion and generate new relativistic electron seeds due to the photoelectric absorption in air. The presented model results agree with the observational and experimental evidence indicating that TGFs are associated with steps of negative lightning leaders and originate from relatively compact regions of space with spatial extent on the order of 10–100 m. The mechanism is not sensitive to the origin and amount of the initial runaway electrons and identical results are obtained whether the initial seeds are provided by the natural background as cosmic ray secondaries or generated by the streamer discharges. We also provide quantitative evidence that in the presence of electrodes the same amplification mechanism and X-ray production may involve generation of runaway electrons from the cathode material. These effects may be relevant to development of new X-ray sources.

1. Introduction

Terrestrial gamma ray flashes (TGFs) (Fishman et al., 1994) represent a spectacular naturally occurring high energy phenomenon in the Earth's atmosphere. These events contain photons with several tens of mega electron-volt energies and likely involve large quantities of energetic electrons, sharing the same physical origin as X-rays generated by laboratory sparks (Stankevich & Kalinin, 1967) or originating from stepping lightning leaders (Moore et al., 2001). Dwyer et al. (2012) provide a review of principal physical processes and experimental findings on TGFs and related phenomena.

It has been discovered by Dwyer (2003) that in order to explain observed intensities of TGFs a feedback mechanism should be involved in these events when an avalanche of relativistic electrons launches positrons and X-rays backwards at its origin to provide additional seeding and replenishment of the avalanche. Dwyer (2003) noted a physical analogy between this relativistic feedback mechanism and feedback mechanisms in conventional Townsend discharges involving positive ions and optical photons. The self-consistent modeling of a large scale streamer (domain size ~5 km) and related space charge effects driven by the relativistic feedback discharges in air around 11–12 km altitudes have been reported by Dwyer (2012) and Liu and Dwyer (2013). It has been

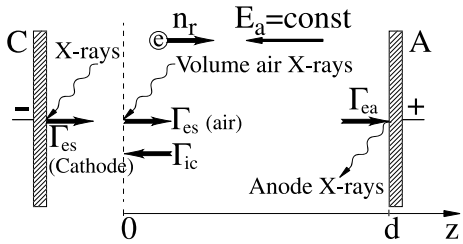

Figure 1. Schematics of one-dimensional simulation domain and principal physical processes.

demonstrated that the relativistic feedback mechanism leads to amplification of the relativistic runaway avalanches allowing to explain observed features of TGFs, including their intensities and pulsing (Dwyer, 2003, 2012; Liu & Dwyer, 2013).

The existing evidence indicates that TGFs are closely associated with intra-cloud leader development and, in particular, with steps of negative lightning leaders (Heumesser et al., 2021; Kohn et al., 2020; Lu et al., 2010, and references cited therein). The processes leading to electric field enhancement around leader tip are therefore likely to play a role in TGF production. A streamer zone of a high potential (~100 MV) lightning leader tip would not exceed several tens of meters (referring to values at sea-level air pressure), and it is reasonable to hypothesize that TGFs should originate from these relatively confined regions of space.

Photoionization of molecular oxygen due to extreme ultraviolet emissions from molecular nitrogen, N_2, in the wavelength range 98–102.5 nm (Zheleznyak et al., 1982) is a fundamental process in positive corona discharges in air where electrons avalanche toward a sharp point that focuses electric field lines leading to significant field enhancements and electron multiplication due to electron impact ionization (Naidis, 1987). In a positive corona system the avalanche of electrons in bulk of discharge volume is initiated by specific distribution of photoionization far away from region of maximum electron density near the electrode where those photons are emitted (Naidis, 2005). There is a direct analogy between this photoionization feedback that occurs in the positive corona discharges in air and the relativistic feedback mechanism proposed by Dwyer (2003). The conditions for inception of relativistic runaway discharges in air, however, have not been defined using the same methodology as in the present literature on conventional positive corona discharges in air (Benilov et al., 2021; Naidis, 2005, and references therein). The definition of these conditions at small spatial scales ≤10–100 m (referring to dimensions of lightning leader streamer zones at sea-level pressure in air) represents a goal of this work.

2. Model Formulation

We note that the relativistic feedback problem is simpler than that of conventional positive corona in air in a sense that it does not contain non-similarity behavior introduced by the quenching of singlet states of molecular nitrogen responsible for photoionization in air (e.g., Naidis, 2005). In Pasko et al. (2022) we developed stationary and time dependent positive corona models in planar and spherical geometry and repeated previously published results on inception of positive corona discharges in air (Naidis, 2005). In this work we extend this modeling to the relativistic feedback problem. Following the convention in the corona literature we use a scaling factor $\delta = n/n_0$, where n is air number density and $n_0 = 2.688 \times 10^{25}$ m^{-3} is a reference value corresponding to standard atmospheric conditions at sea-level in the Earth's atmosphere. We express results in terms of the reduced applied electric field E_0/δ required for the inception of self-sustained relativistic runaway discharges in air versus the reduced physical dimension of space over which this electric field is applied, that is, $d\delta$, where d denotes the gap size.

The geometry of this one dimensional coordinate z dependent model is depicted in Figure 1. The relativistic runaway electrons avalanche in discharge volume and emit the bremsstrahlung X-rays due to their interactions with air and anode material. The presence of anode and cathode electrodes is optional. The flux of electrons bombarding the anode is schematically shown as Γ_{ea}. The X-rays are attenuated due to the photoelectric absorption, Compton scattering, and pair production. The secondary relativistic runaway electrons are produced due to photoelectric absorption of X-rays in the volume of air and from the cathode (both processes are schematically depicted by Γ_{es} fluxes in Figure 1). In this process the photon energy is completely transformed into the electron energy, and the angular distribution of electrons is determined by the corresponding differential scattering cross section (e.g., Carron, 2007, p. 44). Under the self-sustained steady state conditions, the photoelectric feedback produces just enough secondary runaway electrons upstream of the avalanche to replicate constant Γ_{ea}. The processes are analogical to the photoionization feedback in positive corona where each electron arriving at the anode creates on average just enough seed electrons in discharge volume through the photoionization to replicate itself (Naidis, 2005). Under these steady state conditions in the corona and in the relativistic feedback system one can introduce an effective surface anywhere in discharge volume (shown by vertical dashed line in

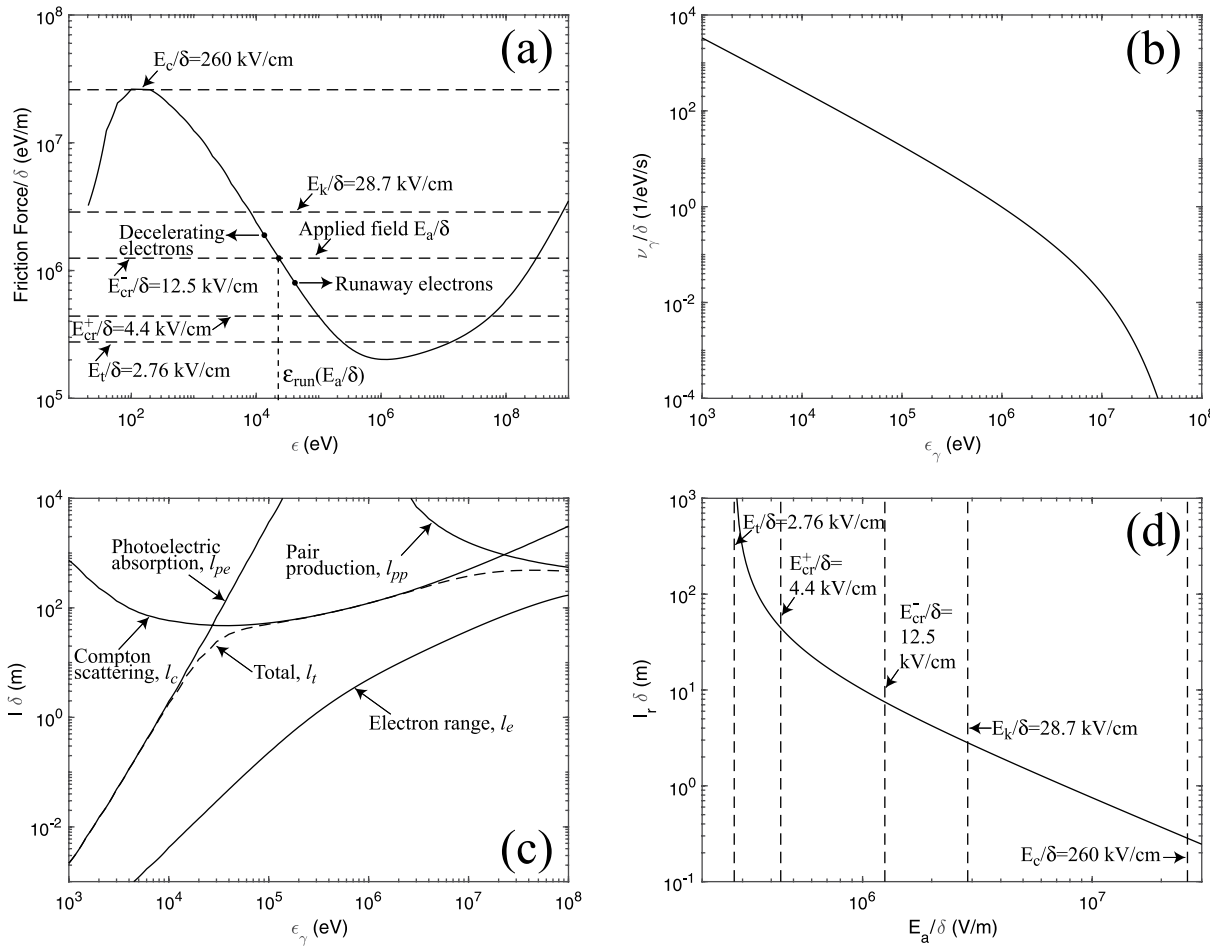

Figure 2. (a) Dynamic friction force on electrons in air; (b) Energy spectrum of X-rays produced by relativistic runaway electrons in air; (c) Attenuation lengths of photons and electrons in air; (d) Avalanche length of relativistic runaway electrons in air.

Figure 1) and express the relationship between ion flux at that location Γ_{ic} and Γ_{es} as $\Gamma_{es} = \gamma_{se}\Gamma_{ic}$, where γ_{se} is the effective secondary electron emission coefficient due to volume photoionization in the positive corona system (Kaptzov, 1950, p. 610) or due to the photoelectric effect in the relativistic electron feedback system. The relation $\Gamma_{es} = \gamma_{se}\Gamma_{ic}$ provides a physically transparent connection to secondary electron emission from cathode surface due to the ion bombardment in conventional Townsend discharge theory. The ion flux Γ_{ic} and the effective coefficient γ_{se}, however, are generally not needed for solution of the corona (Naidis, 2005) or the relativistic feedback problems.

2.1. Runaway Electrons in Air

Figure 2a depicts the friction force acting on electrons in air against the accelerating force from the externally applied field. The format of this figure is adopted from (Moss et al., 2006, please also refer to discussion and references therein). The force has units of eV/m and can be directly compared to the applied electric field E_a to provide an intuitively simple insight into the expected motion of electrons at various energies ε. Figure 2a also provides a summary of various electric field thresholds that are important for description of gas discharge phenomena discussed in this paper: the thermal runaway threshold $E_c/\delta \simeq 260$ kV/cm (Gurevich, 1961), the conventional breakdown field $E_k/\delta = 28.7$ kV/cm defined by the equality of the ionization and dissociative attachment coefficients in air following models of these processes proposed by Morrow and Lowke (1997), and the minimum electric field required for development of relativistic runaway electron avalanche $E_t/\delta = 2.76$ kV/cm (see Coleman & Dwyer, 2006; Dwyer, 2003; Dwyer et al., 2012; Gurevich et al., 1992, and discussion therein). If electrons possess significant energy above ~100 eV corresponding to the E_c peak, they can continue to gain

energy (runaway) in relatively low applied fields $E_t < E_a < E_c$. It had been discovered by Gurevich et al. (1992) that a fraction of secondary electrons produced by these runaways also can become runaways themselves leading to an avalanche multiplication of these electrons. The characteristic length quantifying this exponential growth is shown in Figure 2d (Dwyer et al., 2012, and references therein). Figure 2a also includes the electric fields in streamer zones of positive $E_{cr}^{+}/\delta = 4.4$ kV/cm and negative $E_{cr}^{-}/\delta = 12.5$ kV/cm lightning leaders. There are some variations around these numbers in the existing literature, with E_{cr}^{+} typically quoted to be a factor of 2–3 lower than E_{cr}^{-}. For consistency of numerical estimates we adopt the listed values, which were also used in previous publications (Celestin & Pasko, 2011; Moss et al., 2006). For an example of applied electric field $E_a = E_{cr}^{-}$ shown in Figure 2a electrons with initial energy $\varepsilon < \varepsilon_{run}(E_a) \sim 20$ keV will decelerate, and those with $\varepsilon > \varepsilon_{run}(E_a)$ will gain more energy from electric field than they lose in collisions and will become runaway electrons.

The relativistic runaway electrons with number density n_r and with normalized to unity energy distribution function $f_e(\varepsilon) = \frac{1}{\mathcal{E}_0} e^{-\frac{\varepsilon}{\mathcal{E}_0}}$ (Figure S1a in Supporting Information S1) (where $\mathcal{E}_0 = 7.3 \times 10^6$ eV) (Dwyer et al., 2012, and references therein) avalanche against the constant applied electric field with magnitude E_a, and their avalanche multiplication is characterized by length shown in Figure 2d, $l_r\delta = \frac{1}{E_a/\delta} \frac{\mathcal{E}_0}{\left(1-\frac{E_{t0}}{E_a/\delta}\right)}$ (Dwyer et al., 2012, and references therein), where $E_{t0} = 2.76 \times 10^5$ V/m corresponds to the sea-level pressure E_t value shown in Figure 2a. The deflection of electrons by nuclei of oxygen and nitrogen atoms in air leads to braking (bremsstrahlung) radiation characterized by the energy spectrum shown in Figure 2b. Due to the $1/\varepsilon_\gamma$ dependence of the related cross section, the distribution is characterized by orders of magnitude higher number of photons at low energies 1–100 keV than around the $\mathcal{E}_0$ threshold. These photons are attenuated as they propagate in air due to photoelectric absorption, Compton scattering, and pair production. The corresponding attenuation lengths are shown in Figure 2c. For the spatial scales $l\delta \leq 100$ m of interest in present work the attenuation is dominated by photoelectric absorption and Compton scattering. At energies above ~1 keV the electron emerging as a result of photoelectric absorption of a photon with energy ε_γ carries essentially the same energy as photon energy (minus a small binding energy increment), that is, $\varepsilon \simeq \varepsilon_\gamma$. The photoelectric absorption is the primary process that can effectively produce runaway electrons on spatial scales of interest in this work and in a given electric field E_a as soon as the condition $\varepsilon > \varepsilon_{run}(E_a)$ is satisfied (see Figure 2a).

The relativistic runaway electrons are described by linear equation ($n_r \propto S_{pe}$):

$$\nabla \cdot \left(n_r \vec{c}\right) = \alpha_r n_r c + S_{pe} \tag{1}$$

where the ionization coefficient $\alpha_r = l_r^{-1}$ [m^{-1}], c is speed of light in free space and the source term S_{pe} describes production of runaway electrons due to the photoelectric effect. For a case when $S_{pe} = S_0$ with S_0 being a constant background rate of production of runaway electrons, the equation has a one-dimensional (coordinate z dependent) solution: $n_r(z) = \frac{S_0 l_r}{c}\left(e^{\frac{z}{l_r}} - 1\right)$. For $z \ll l_r$, $n_r(z) \simeq \frac{S_0 z}{c}$ and for $z \gg l_r$, $n_r(z) = n_{r_0} e^{\frac{z}{l_r}}$, where $n_{r_0} = \frac{S_0 l_r}{c}$. This emphasizes that runaway electrons arriving at the end of model region after many multiplications (i.e., at the anode) are mostly defined by their seeds in a relatively narrow region of space with size l_r. We also note that similarly to positive corona system (Naidis, 2005), the seed runaway electrons due to the photoelectric effect are mostly produced by the region of maximum density of runaway electrons at the end of the multiplication region. The solution of the photoelectric feedback problem requires finding a specific value of applied electric field $E_a = E_0$ and related self-consistent distribution of $S_{pe}(z)$ that provides full self-replication of runaway electrons. The constant background rate S_0 is generally not needed for the solution of the feedback problem, however, it can represent initial runaway seeds in the form of cosmic ray secondaries with typical values at lightning initiation altitudes being $S_0 = 10$ m^{-3}s^{-1} (McCarthy & Parks, 1992), or a production of runaway electrons in the regions populated by propagating streamers (Celestin & Pasko, 2011; Moss et al., 2006). This discussion also emphasizes that even under conditions when $E_a < E_0$, if $S_0 > 0$ there is a steady state solution and a significant exponential multiplication of runaway electrons.

2.2. Photoelectric Runaway Electrons Due To X-Rays

The X-ray generation by runaway electrons in air is characterized by doubly differential cross-section of the bremsstrahlung photon production $\frac{d^2\sigma_{br}}{d\varepsilon_\gamma d\Omega}$, where the angular dependence is the one for the emitted photon

(Heitler, 1954, p. 245; Lehtinen, 2000, p. 45, and references therein). The X-ray emission frequency per unit energy per one runaway electron [1/eV/s] (Figure 2b) is:

$$\nu_\gamma(\varepsilon_\gamma) = 2n \int_{\varepsilon_\gamma}^{\infty} f_e(\varepsilon) \frac{d\sigma_{\rm br}}{d\varepsilon_\gamma}(\varepsilon, \varepsilon_\gamma) \upsilon(\varepsilon) d\varepsilon \tag{2}$$

where $\upsilon(\varepsilon) = c\sqrt{1-(1+\varepsilon/(mc^2))^{-2}}$, m is electron rest mass, and $\frac{d\sigma_{\rm br}}{d\varepsilon_\gamma} = \int_\Omega \frac{d^2\sigma_{br}}{d\varepsilon_\gamma d\Omega}\, d\Omega$. The total emission frequency of bremsstrahlung photons per one runaway electron [1/s] is $\nu_\gamma^t = \int \nu_\gamma(\varepsilon_\gamma) d\varepsilon_\gamma$, where integration is performed over the energy interval 1 keV to 100 MeV shown in Figure 2b ($\nu_\gamma^t/\delta = 1.67 \times 10^7 {\rm s}^{-1}$). In the following we refer to these X-rays as air X-rays. As will be emphasized further the bremsstrahlung photon production scales quadratically with atomic number Z and in our representative calculations we will include tungsten (W) and aluminum (Al) as representative high and low Z materials ($Z_{\rm N} = 7$ and $Z_{\rm O} = 8$ in air, $Z_{\rm Al} = 13$, and $Z_{\rm W} = 73$).

The number of runaway electrons produced per unit volume per second due to photoelectric effect in air due to air X-rays:

$$S_{\rm pe}^{\rm air-X}(\vec{r}) = \int_{\epsilon_{\rm run}(E_{\rm a})}^{\infty} \int_{V'} \xi_{\rm pe} \nu_\gamma(\varepsilon_\gamma) n_{\rm r}(\vec{r}') e^{-k_{\rm t}(\varepsilon_\gamma)R} \frac{n\sigma_{\rm pe}(\varepsilon_\gamma)}{4\pi R^2} dV' d\varepsilon_\gamma \tag{3}$$

where $R = |\vec{r} - \vec{r}'|$ is the distance between point of source $\vec{r}'$ and point of observation $\vec{r}$, $k_{\rm t} = n(\sigma_{\rm pe} + \sigma_{\rm c} + \sigma_{\rm pp})$ is the total absorption coefficient including the photoelectric absorption, Compton scattering, and pair production in air, with respective cross sections $\sigma_{\rm pe}$, $\sigma_{\rm c}$, and $\sigma_{\rm pp}$, and the quantity $\xi_{\rm pe} = 5 \times 10^{-3}$ denotes efficiency of production of runaway electrons accounting for the differential cross sections of the bremsstrahlung radiation and the production of electrons due to the photoelectric absorption (see Discussion section). The structure of Equation 3 accounts for volumetric emission source of photons, geometrical spreading and attenuation of photons as they propagate, and their absorption by target molecules, similarly to a formulation used for photoionization problems (e.g., Janalizadeh & Pasko, 2019, and references therein). The effects of bremsstrahlung induced photoionization on the propagation of positive streamers in different N_2/O_2 mixtures have been discussed by Kohn et al. (2017). Figure 2c illustrates the characteristic absorption lengths of photoelectric absorption $l_{\rm pe} = 1/(n\sigma_{\rm pe})$, Compton scattering $l_{\rm c} = 1/(n\sigma_{\rm c})$, pair production $l_{\rm pp} = 1/(n\sigma_{\rm pp})$, and total absorption $l_{\rm t} = 1/k_{\rm t}$. For comparison Figure 2c also shows the electron range $l_{\rm e}$ over the same energy range. The photon cross sectional data are taken from http://www.nist.gov/pml/data/xcom. The electron range data are from https://physics.nist.gov/PhysRefData/Star/Text/ESTAR.html. We solve Equation 3 by replacing it with an equivalent set of Helmholtz equations (Bourdon et al., 2007; Janalizadeh & Pasko, 2019) (with details of numerical implementation provided in Supplementary Information).

The photoelectric runaway electrons in air are also produced due to X-rays emitted by the anode upon bombardment by runaway electrons $S_{\rm pe}^{\rm anode-X}(\vec{r})$. We consider aluminum (Al) and tungsten (W) as two representative electrode materials. The total number of runaway electrons produced per unit volume per unit time in air due to the photoelectric absorption is then $S_{\rm pe}(\vec{r}) = S_{\rm pe}^{\rm air-X}(\vec{r}) + S_{\rm pe}^{\rm anode-X}(\vec{r})$. The runaway electrons are also emitted from the cathode due to the air and anode X-rays. Both Al and W materials have a factor of 10^3 higher mass densities as compared to air at sea-level pressure. The bremsstrahlung photon production from tungsten is enhanced by a factor of 10^2 due to Z^2 scaling of the related cross section. In comparison to air tungsten also has a factor of 10^4 higher cross section for photoelectric absorption. The calculations follow the integral approach defined in Equation 3 by replacing the X-ray source in air $\nu_\gamma(\varepsilon_\gamma)$ with corresponding quantities defined for aluminum and tungsten $\nu_\gamma^{\rm Al,W}(\varepsilon_\gamma)$, and the photoelectric absorption cross section in air $\sigma_{\rm pe}(\varepsilon_\gamma)$ with corresponding Al and W cross sections $\sigma_{\rm pe}^{\rm Al,W}(\varepsilon_\gamma)$ (details of numerical implementation are provided in Supplementary Information).

3. Results

The differential Equation 1 and integral Equation 3 are self-consistently solved for $n_{\rm r}$ and $S_{\rm pe}$, respectively. The threshold electric field E_0 ($E_{\rm t} < E_0 < E_{\rm c}$) required for inception of relativistic runaway discharges for different gap dimensions d is obtained by an iterative process. The solution is started by setting an arbitrary initial value of E_0, initiating a primary relativistic runaway electron avalanche with initial density $n_{\rm rp}(d) = 1\ {\rm m}^{-3}$ at the right boundary of the simulation domain at $z = d$ (Figure 1), and assuming $S_{\rm pe} = 0$ everywhere in the simulation domain. The

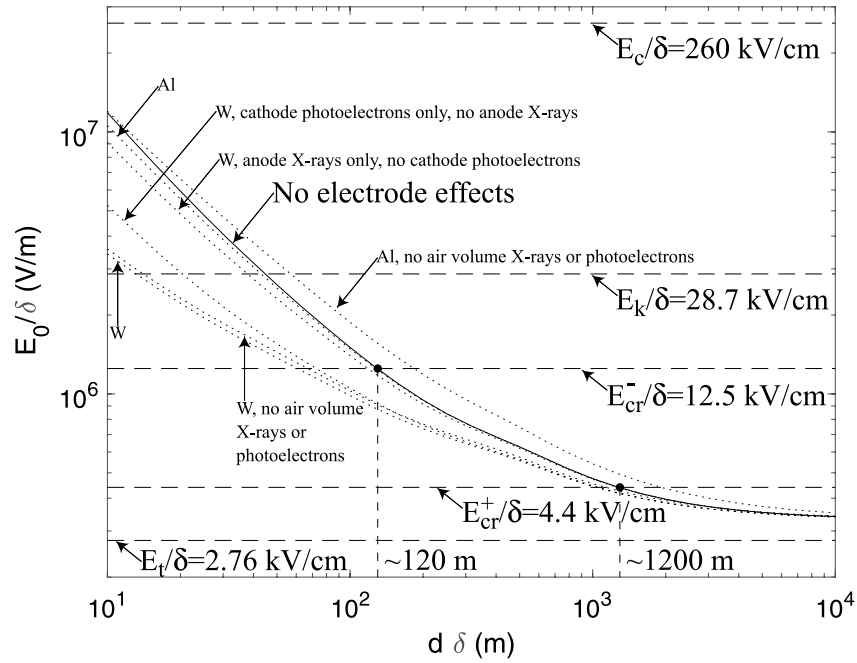

Figure 3. The reduced threshold electric field E_0/δ required for inception of relativistic runaway discharges for different gap sizes $d\delta$ in air.

resultant primary relativistic electron distribution n_{rp} produces photoelectric source of runaway electrons S_{pep} that is used to find the next iteration n_{rs} (with $n_{rp}(d) = 0$). The density n_{rs} produces S_{pes} that gives next iteration n_{rss}. The final E_0 is obtained by simple iterations (by increasing or decreasing E_0) until the volume integrated n_{rs} and n_{rss} agree. Specific spatial distributions are illustrated in Figure S3 in Supporting Information S1. Due to the linear dependence of n_r on S_{pe} and vice versa, the results do not depend on the specific value $n_{rp}(d) = 1\ \mathrm{m}^{-3}$. The solutions identical to those shown in Figure 3 are also produced by assuming $n_{rp}(d) = 0$ and initiating the iterations with an arbitrary constant value of $S_{pe} = S_0$. Figure 3 shows the resultant E_0 as a function of d, in reduced form.

The no electrode effects solution shown in Figure 3 gives the size of the region and the electric field value in that region that is required for inception of relativistic runaway discharges. As discussed in the model formulation section for any d and for corresponding $E_a < E_0$ there is a stationary (if $S_0 \neq 0$), or a damped solution, depending on external sources of runaway electrons. For $E_a > E_0$ the system can be initiated by a single runaway electron and leads to very fast multiplication of electrons developing on time scales on the order of d/c. In the conventional positive corona system the $E_a > E_0$ regime is accompanied by growth of electron density that is normally bounded by outflow of plasma through chamber walls containing the discharge, or by space charge effects modifying the applied field E_a (Benilov et al., 2021). The gap sizes and electric fields in Figure 3 provide sufficient potential drops for the runaway distribution with $\mathcal{E}_0 = 7.3 \times 10^6$ eV cutoff to be valid. The softer distributions are expected at reduced gap sizes and potential differences (<100 MV) (Celestin et al., 2015).

Under thundercloud conditions there are three principal pathways by which the relativistic feedback discharges can operate: (a) The local electric field staying below the E_0 threshold over physical space with dimension d, with no lightning leaders developed yet, but with streamer activity possibly present due to hydrometeors and their collisions (Jansky & Pasko, 2020, and references therein); (b) the increase of local electric field over the E_0 threshold over physical space with dimension d, and similarly to the previous scenario, with no leaders but possibly with streamers present; (c) A bi-directional IC leader discharge propagating and creating extensive regions of quasi-constant electric fields E_{cr}^- and E_{cr}^+ in respective negative and positive streamer zones.

The first scenario is expected to be of the most common occurrence in a typical thundercloud environment and may lead to quasi-stationary solutions and long duration X-ray emissions discussed in the model formulation section. These emissions should cease immediately following the lightning discharge removing the charge separation regions that created the initial high field enhancements (Eack & Beasley, 2015; McCarthy & Parks, 1992, and references therein).

The second scenario would likely result in an abrupt growth of plasma conductivity and space charge effects similar to those modeled in (Dwyer, 2012; Liu & Dwyer, 2013), but on smaller scales of 10–100 m driven by the photoelectric feedback and leading to lightning leader initiation (Liu et al., 2022; Stolzenburg et al., 2013). Depending on number of seed electrons (i.e., produced by streamers (Celestin & Pasko, 2011)) the elementary time scale of this process is defined by several round trips with speed of light over $d\delta \simeq$ 10–100 m, i.e., (0.066–0.66)/δ μs in good agreement with 10 μs narrow bipolar events (NBEs) (Tilles et al., 2020).

For the third scenario, the branches of lightning leaders significantly modify the externally applied electric field as they focus electric field lines on their tips and therefore effectively screen (i.e., reduce) electric field in other regions of space. In the negative leader stepping process (during the negative corona flashes) the field of highly conducting negative leader tip is temporarily unshielded and can reach values significantly exceeding the conventional threshold E_k (E_k is included for the reference in Figure 3). For low potential leaders with a streamer zone size $R_{st}^{-}\delta \leq$10 m, the field near the negative tip can reach $1.5E_k$ (Bazelyan & Raizer, 2000, p. 68). The analysis presented in (Celestin & Pasko, 2011, Figure 7, and discussion therein) indicates that with an increase of the leader potential and for $R_{st}^{-}\delta \sim \delta$100 m this field moves closer to E_k. In both cases, however, this high field $E \geq E_k$ only exists several centimeters from the leader tip and can not be sustained over dδ = 20–40 m required for the open air inception of the relativistic runaway discharge in accordance with Figure 3. For a leader tip potential U_l the sizes of negative and positive streamer zones can be evaluated as $R_{st}^{-} = U_l/(2E_{cr}^{-})$ and $R_{st}^{+} = U_l/\left(2E_{cr}^{+}\right)$, respectively (see Celestin & Pasko, 2011; Moss et al., 2006, and discussion therein). For a leader with $U_l = 10$ MV the streamer zone has spatial extent $R_{st}^{-}\delta = 4$ m. For a high potential leader with $U_l = 300$ MV that leads to TGFs (Mallios et al., 2013) $R_{st}^{-}\delta = 120$ m. At a representative 11 km TGF altitude $\delta \simeq 0.275$ and $R_{st}^{-} = 436$ m. The speed of light round trip over 436 m is ∼3 μs indicating that ∼50 μs energetic in-cloud pulses (EIPs) require several round trips before high-fluence TGFs are produced (Tilles et al., 2020). The smooth EIP sferics may represent the manifestation of relatively large volume of growing conductivity and current as opposed to the very high frequency (VHF) noisy streamers expected to coexist in the same physical space (Tilles et al., 2020). The 10–50 μs are broadly consistent with times required for runaway electrons producing streamers to traverse the above mentioned spatial scales. The quantitative modeling of related processes indicates that slow low-frequency (LF) pulses are likely generated directly by the TGF sources (Berge et al., 2022). It can be seen from Figure 3 that as soon as the streamer zone size reaches the threshold $d\delta \simeq 100$ m for negative leader tip and $d\delta \simeq 1{,}000$ m for positive leader tip the inception conditions for the relativistic runaway discharge will be satisfied. Since both positive and negative streamer zone sizes scale with field as $1/E$ and the required gap size for the relativistic feedback drops faster than $1/E^2$ (see Figure 3), for any given leader with potential U_l the conditions for relativistic runaway discharge will always be first satisfied in the negative streamer zone. We associate the situation when the negative streamer zone reaches this threshold with a condition when terrestrial gamma ray flash is produced by stepping lightning leaders. The occurrence of TGFs in association with positive leaders is not excluded but is rare (Hare et al., 2016).

Although representing a bi-directional leader as a long unbranched conductor is a reasonable approximation that provides insight into the leader fields observed experimentally (Pasko, 2014), the actual leaders exhibit significant branching with VHF dark positive leaders developing extensive networks before development of negative leader branches (Boggs et al., 2022; Mallios et al., 2013). The potential drop in each branch decreases after the branching (Celestin & Pasko, 2011). For branched leaders the length of the streamer zone would not necessarily satisfy the relativistic runaway condition during each step (i.e., the leader may continue stepping propagation without producing TGFs (Cummer et al., 2015)). The amplification of runaway avalanches even under conditions when $E_a < E_0$ may lead to observable X-ray emissions from leader streamer zones (Moore et al., 2001), up to fluences approaching TGFs (Celestin et al., 2015).

4. Discussion

Figure 3 provides illustration of effects produced by model electrodes made of aluminum or tungsten (Figure 1). For simplicity for cases considered it is assumed that the same material is used for both cathode and anode. As noted in the model formulation section, the principal effects produced by electrodes include X-ray production from the anode upon bombardment by runaway electrons, and the production of relativistic runaway electrons from the cathode due to the photoelectric effect. Figure 3 indicates that aluminum (being a low atomic number material) does not significantly modify the open air solutions. The tungsten solutions significantly modify the E_0

threshold by lowering it to values slightly above and below the E_k value for small gap sizes $d\delta \sim 10$ m. Consistent with discussion in the model formulation section, the seed runaway electrons released from the cathode play the dominant role in comparison with effects of X-rays emitted from the anode. Although these results are obtained for highly simplified planar geometry, they indicate a potential importance of the electrode material and configuration for interpretation of X-ray production from laboratory sparks (see discussion by da Silva et al. (2017), Parkevich et al. (2022), Stankevich and Kalinin (1967), and extensive list of references therein). The buildup of runaway electrons in the discharge volume may not be easily observed due to bright streamer, pilot and leader activity. However, related conductivity changes may be responsible for the observed correlation of X-ray fluxes and the cathode current pulses (Kochkin et al., 2015). It is remarkable that even in a case when no air volume X-rays and photoelectrons are produced (in the model these processes can be simply switched off), the relativistic electron runaway feedback with low E_0 threshold exists solely due to the production of relativistic electrons from the cathode due to X-rays emitted by the anode (please refer to the no air volume X-rays or photoelectrons solutions shown in Figure 3). In the present modeling we exclude effects related to Compton back scattering of X-rays from the cathode and also production of the characteristic (K_α) X-rays from the cathode and anode. The K absorption edge for tungsten, for example, is ~58 keV. These photons emerging from the cathode in the same direction as the runaway avalanche can provide an efficient additional channel for seed runaway electrons through either photoelectric absorption, Compton scattering or pair production (we note that at ~5 MeV pair production in tungsten is comparable to Compton scattering).

The Compton scattering and pair production in air are included in the present modeling as photon attenuation processes but not as processes leading to generation of feedback runaway electrons. As indicated by data shown in Figure 2c the Compton scattering interaction has a characteristic distance $l_c\delta$ of approximately 100 m over the 10–100 keV range of energies, which are of primary interest in this work. As demonstrated above, in order for the feedback process to be effective, the seed runaway electrons should be produced in the relatively narrow region with characteristic length l_r upstream from the avalanche. The values of $l_r\delta$ shown in Figure 2b indicate that for the fields E_{cr}^- and E_{cr}^+ of primary interest in this work, the 100 m Compton range $l_c\delta$ appears to significantly exceed $l_r\delta$ (i.e., $l_r\delta \sim 7$ m at $E_a = E_{cr}^-$). Furthermore, the kinematics of Compton scattering only produce electrons in the forward direction with respect to the incoming photon, and the backward moving bremsstrahlung photons produced by the relativistic runaway avalanche would preferentially produce electrons that would move against the primary runaway avalanche, decelerate, and would need to experience additional scattering interactions to become a part of the runaway population. The backward moving bremsstrahlung photons can Compton backscatter ($\theta = \pi$) and depending on their incoming energy ε_γ with respect to the electron rest energy mc^2 would possess significant energy $\varepsilon'_\gamma \le mc^2/2 = 255$ keV ($\varepsilon'_\gamma = mc^2/(2 + mc^2/\varepsilon_\gamma)$). These photons with energy ε'_γ can contribute to the runaway population by both photoelectric absorption and Compton scattering. However, due to the original Compton scattering event having low probability and long range $l_c\delta \ge 100$ m (i.e., $l_c\delta > l_r\delta$), we consider these effects as not dominant producers of feedback runaway electrons. On the same physical grounds we exclude pair production, and for the considered reduced $d\delta$ scales of interest, that is, 10–100 m, retain only the photoelectric absorption as the dominant relativistic feedback factor.

Having considered $l_c\delta$ and $l_{pp}\delta$ in Figure 2c, the Compton scattering and pair production are important feedback factors for $d\delta$ values ~1–10 km (Dwyer, 2012; Liu & Dwyer, 2013). Our model values of E_0/δ at these scales are generally higher than those shown by Dwyer (2003), Figure 3 and Skeltved et al. (2014), Figure 6, and this could be attributed to the contribution of Compton scattering and pair production on these scales. In the $d\delta$ range of 10–100 m the open air onset values obtained in this work are a factor of 2 higher than those reported by Dwyer (2003), Figure 3 and Skeltved et al. (2014), Figure 6, and this can be attributed to these authors employing the simulation domain with 10 km vertical extent filled with air at sea-level pressure leading to reduction of range scales and therefore overestimation of frequencies of all physical interactions by up to a factor of 3. Additionally, for the 10 km, the speed of light round trip time is $66/\delta$ μs leading to modeled TGF pulse durations on the order of 1 ms (Dwyer, 2012; Liu & Dwyer, 2013) significantly exceeding the observed ~10 μs and ~50 μs durations of NBEs and EIPs, respectively (Tilles et al., 2020), and slow LF pulses (Berge et al., 2022).

The number of relativistic runaway electrons created by the photoelectric absorption is controlled by two principal factors: (a) the differential cross sections of the bremsstrahlung photons and photoelectrons (Figure S2 in Supporting Information S1); (b) the applied field E_a dependent extent of energy interval (from $\varepsilon_{run}(E_a)$ to ∞) in which electron can gain energy and runaway (Figure 2a). For the first factor, the bremsstrahlung photons that facilitate feedback are launched backwards with respect to the avalanching runaway electrons. In order to

contribute to the avalanche the runaway electron produced by these photons should be launched in the direction of the avalanche (i.e., in the range of angles $\pi/2 < \theta < \pi$, where θ is measured from the photon direction). As evident from Figure S2a in Supporting Information S1, an isotropic approximation for the bremsstrahlung photons is a good approximation at low energies ≤100 keV, with the backscattering reduced at higher energies. The backscattering variation for the photoelectric electrons illustrated in Figure S2b in Supporting Information S1 is even sharper, indicating, in particular, over an order of magnitude reduction at $\theta = 3\pi/4$ (135°) at 1 MeV with respect to the 10 keV value. We note that the lower runaway bound energies $\varepsilon_{run}(E_a)$ for the fields E_{cr}^- and E_{cr}^+ of primary interest in this work reside in the 10–100 keV range (see Figure 2a) and the discussion above clearly indicates that both cross sections are highly anisotropic at these energies. To account for the reduction in the production runaway electrons due to these anisotropies we introduced in the model formulation an efficiency parameter $\xi_{pe} = 5 \times 10^{-3}$. The model results appeared to be relatively insensitive to this parameter. In particular, at $d\delta = 100$ m the increase to $\xi_{pe} = 5 \times 10^{-2}$ or reduction to $\xi_{pe} = 5 \times 10^{-4}$ led only to ∼13% variations in E_0 values shown in Figure 3, not affecting any principal conclusions of this work. At $d\delta = 1{,}000$ m the same changes resulted in ∼4% variations. The second factor (the energy interval available for electron to runaway) practically involves the energies from $\varepsilon_{run}(E_a)$ to the $\mathcal{E}_0$ cutoff defining sharp drop off of $\nu_\gamma(\varepsilon_\gamma)$ at high energies (Figure 2b). The effects related to this factor are accurately included in present modeling and depending on specific range R and air pressure p can exhibit up to eight orders of magnitude variations accounted by the propagator functions (Figure S1b in Supporting Information S1).

5. Conclusions

The photoelectric absorption plays a dominant role in feedback amplification of the relativistic runaway electron avalanches on spatial scales ∼10–100 m in sea-level pressure air in the Earth's atmosphere. Using the same physical methodology as for conventional positive corona discharges in air, the conditions of inception of relativistic runaway discharges in air in terms of gap size, applied electric field and air pressure have been formulated. The results are relevant to understanding of physical conditions required for seeding of high conductivity regions in virgin air leading to lightning leader initiation, and understanding of intense fluxes of gamma rays produced by stepping leaders. The obtained model results indicate, in particular, that TGFs observed in association with stepping of negative lightning leaders can be explained by the spatial growth of the leader streamer zone, and a significant and source independent multiplication of relativistic runaway electrons occurs when a threshold of approximately 100 m (for standard air pressure conditions at sea-level) is reached. Below this threshold, the dominant seeding mechanism of runaway electrons is the thermal runaway electron production by streamers. A similar feedback amplification produced by the photoelectric absorption and generation of runaway electrons from the cathode material may be relevant to explanation of observed X-ray emissions from centimeter to meter long sparks under laboratory conditions.

Data Availability Statement

The original data presented in this paper as figures may be downloaded from the link https://doi.org/10.26208/5SGE-R820.

Acknowledgments
This research has been supported by the NSF grants AGS-1744099 and AGS-2010088 to Penn State University. S Celestin acknowledges support from the French space agency (CNES) within the projects OREO and STRATELEC, and by the Institut Universitaire de France (IUF). J Jansky gratefully acknowledges financial support from the grant VAROPS (DZRO FVT 3) granted by the Ministry of Defense of the Czech Republic. This study was conducted during a sabbatical visit of V P Pasko to the Plasma Physics Laboratory (LPP), Ecole Polytechnique, Palaiseau, France, and to the Laboratory of Physics and Chemistry of the Environment and Space (LPC2E), University of Orleans, France in the Fall of 2022. Hospitality of colleagues and staff at LPP and LPC2E is gratefully acknowledged.

References

Bazelyan, E. M., & Raizer, Y. P. (2000). *Lightning physics and lightning protection*. IoP Publishing Ltd.

Benilov, M. S., Almeida, P. G. C., Ferreira, N. G. C., Almeida, R. M. S., & Naidis, G. V. (2021). A practical guide to modeling low-current quasi-stationary gas discharges: Eigenvalue, stationary, and time-dependent solvers. *Journal of Applied Physics*, *130*(12), 121101. https://doi.org/10.1063/5.0057856

Berge, N., Celestin, S., Garnung, M. B., Xu, W., Marshall, R. A., & Cummer, S. A. (2022). Modeling low-frequency radio emissions from terrestrial gamma ray flash sources. *Journal of Geophysical Research*, *127*(5), e2021JD036040. https://doi.org/10.1029/2021JD036040

Boggs, L. D., Mach, D., Bruning, E., Liu, N., van der Velde, O. A., Montanya, J., et al. (2022). Upward propagation of gigantic jets revealed by 3D radio and optical mapping. *Science Advances*, *8*(31), eabl8731. https://doi.org/10.1126/sciadv.abl8731

Bourdon, A., Pasko, V. P., Liu, N. Y., Celestin, S., Segur, P., & Marode, E. (2007). Efficient models for photoionization produced by non-thermal gas discharges in air based on radiative transfer and the Helmholtz equations. *Plasma Sources Science and Technology*, *16*(3), 656–678. https://doi.org/10.1088/0963-0252/16/3/026

Carron, N. J. (2007). *An introduction to the passage of energetic particles through matter*. Taylor and Francis.

Celestin, S., & Pasko, V. P. (2011). Energy and fluxes of thermal runaway electrons produced by exponential growth of streamers during the stepping of lightning leaders and in transient luminous events. *Journal of Geophysical Research*, *116*(A3), A03315. https://doi.org/10.1029/2010ja016260

Celestin, S., Xu, W., & Pasko, V. P. (2015). Variability in fluence and spectrum of high-energy photon bursts produced by lightning leaders. *Journal of Geophysical Research*, *120*(12), 10712–10723. https://doi.org/10.1002/2015JA021410

Coleman, L. M., & Dwyer, J. R. (2006). Propagation speed of runaway electron avalanches. *Geophysical Research Letters*, *33*(11), L11810. https://doi.org/10.1029/2006GL025863

Cummer, S. A., Lyu, F., Briggs, M. S., Fitzpatrick, G., Roberts, O. J., & Dwyer, J. R. (2015). Lightning leader altitude progression in terrestrial gamma-ray flashes. *Geophysical Research Letters*, *42*(18), 7792–7798. https://doi.org/10.1002/2015GL065228

da Silva, C. L., Millan, R. M., McGaw, D. G., Yu, C. T., Putter, A. S., LaBelle, J., & Dwyer, J. (2017). Laboratory measurements of X-Ray emissions from centimeter-long streamer corona discharges. *Geophysical Research Letters*, *44*(21), 11174–11183. https://doi.org/10.1002/2017GL075262

Dwyer, J. R. (2003). A fundamental limit on electric fields in air. *Geophysical Research Letters*, *30*(20), 2055. https://doi.org/10.1029/2003GL017781

Dwyer, J. R. (2012). The relativistic feedback discharge model of terrestrial gamma ray flashes. *Journal of Geophysical Research*, *117*(A2), A02308. https://doi.org/10.1029/2011JA017160

Dwyer, J. R., Smith, D. M., & Cummer, S. A. (2012). High-energy atmospheric physics: Terrestrial gamma-ray flashes and related phenomena. *Space Science Reviews*, *173*(1–4), 133–196. https://doi.org/10.1007/s11214-012-9894-0

Eack, K. B., & Beasley, W. H. (2015). Long-duration X-ray emissions observed in thunderstorms. *Journal of Geophysical Research*, *120*(14), 6887–6897. https://doi.org/10.1002/2015JD023262

Fishman, G. J., Bhat, P. N., Mallozzi, R., Horack, J. M., Koshut, T., Kouveliotou, C., et al. (1994). Discovery of intense gamma-ray flashes of atmospheric origin. *Science*, *264*(5163), 1313–1316. https://doi.org/10.1126/science.264.5163.1313

Gurevich, A. V. (1961). On the theory of runaway electrons. *Soviet Physics JETP*, *12*, 904–912.

Gurevich, A. V., Milikh, G. M., & Roussel-Dupré, R. A. (1992). Runaway electron mechanism of air breakdown and preconditioning during a thunderstorm. *Physics Letters A*, *165*(5–6), 463–468. https://doi.org/10.1016/0375-9601(92)90348-P

Hare, B. M., Uman, M. A., Dwyer, J. R., Jordan, D. M., Biggerstaff, M. I., Caicedo, J. A., et al. (2016). Ground-level observation of a terrestrial gamma ray flash initiated by a triggered lightning. *Journal of Geophysical Research*, *121*(11), 6511–6533. https://doi.org/10.1002/2015JD024426

Heitler, W. (1954). *The quantum theory of radiation* (3rd ed.). Clarendon.

Heumesser, M., Chanrion, O., Neubert, T., Christian, H. J., Dimitriadou, K., Gordillo-Vazquez, F. J., et al. (2021). Spectral observations of optical emissions associated with terrestrial gamma-ray flashes. *Geophysical Research Letters*, *48*(4), e2020GL090700. https://doi.org/10.1029/2020GL090700

Janalizadeh, R., & Pasko, V. P. (2019). A general framework for photoionization calculations applied to nonthermal gas discharges in air. *Plasma Sources Science and Technology*, *28*(10), 105006. https://doi.org/10.1088/1361-6595/ab4374

Jansky, J., & Pasko, V. P. (2020). Modeling of streamer ignition and propagation in the system of two approaching hydrometeors. *Journal of Geophysical Research*, *125*(6), e2019JD031337. https://doi.org/10.1029/2019JD031337

Kaptzov, N. A. (1950). *Elektricheskiye Yavleniya v Gazakh i Vacuume*. GITTL.

Kochkin, P. O., van Deursen, A. P. J., & Ebert, U. (2015). Experimental study on hard X-rays emitted from metre-scale negative discharges in air. *Journal of Physics D: Applied Physics*, *48*(2), 025205. https://doi.org/10.1088/0022-3727/48/2/025205

Kohn, C., Chanrion, O., & Neubert, T. (2017). The influence of bremsstrahlung on electric discharge streamers in N-2, O-2 gas mixtures. *Plasma Sources Science and Technology*, *26*(1), 015006. https://doi.org/10.1088/0963-0252/26/1/015006

Kohn, C., Heumesser, M., Chanrion, O., Nishikawa, K., Reglero, V., & Neubert, T. (2020). The emission of terrestrial gamma ray flashes from encountering streamer coronae associated to the breakdown of lightning leaders. *Geophysical Research Letters*, *47*(20), e2020GL089749. https://doi.org/10.1029/2020GL089749

Lehtinen, N. G. (2000). *Relativistic runaway electrons above thunderstorms*. (Ph.D. thesis). Stanford University.

Liu, N. Y., & Dwyer, J. R. (2013). Modeling terrestrial gamma ray flashes produced by relativistic feedback discharges. *Journal of Geophysical Research*, *118*(5), 2359–2376. https://doi.org/10.1002/jgra.50232

Liu, N. Y., Scholten, O., Hare, B. M., Dwyer, J. R., Sterpka, C. F., Kolmasova, I., & Santolik, O. (2022). LOFAR observations of lightning initial breakdown pulses. *Geophysical Research Letters*, *49*(6), e2022GL098073. https://doi.org/10.1029/2022GL098073

Lu, G., Blakeslee, R. J., Li, J., Smith, D. M., Shao, X. M., McCaul, E. W., et al. (2010). Lightning mapping observation of a terrestrial gamma-ray flash. *Geophysical Research Letters*, *37*(11), L11806. https://doi.org/10.1029/2010GL043494

Mallios, S. A., Celestin, S., & Pasko, V. P. (2013). Production of very high potential differences by intracloud lightning discharges in connection with terrestrial gamma ray flashes. *Journal of Geophysical Research*, *118*(2), 912–918. https://doi.org/10.1002/jgra.50109

McCarthy, M. P., & Parks, G. K. (1992). On the modulation of X-ray fluxes in thunderstorms. *Journal of Geophysical Research*, *97*(D5), 5857–5864. https://doi.org/10.1029/91jd03160

Moore, C. B., Eack, K. B., Aulich, G. D., & Rison, W. (2001). Energetic radiation associated with lightning stepped-leaders. *Geophysical Research Letters*, *28*(11), 2141–2144. https://doi.org/10.1029/2001GL013140

Morrow, R., & Lowke, J. J. (1997). Streamer propagation in air. *Journal of Physics D: Applied Physics*, *30*(4), 614–627. https://doi.org/10.1088/0022-3727/30/4/017

Moss, G. D., Pasko, V. P., Liu, N. Y., & Veronis, G. (2006). Monte Carlo model for analysis of thermal runaway electrons in streamer tips in transient luminous events and streamer zones of lightning leaders. *Journal of Geophysical Research*, *111*(A2), A02307. https://doi.org/10.1029/2005JA011350

Naidis, G. V. (1987). Ignition voltage of a positive corona in air. *Soviet Journal of Plasma Physics*, *13*, 645–648.

Naidis, G. V. (2005). Conditions for inception of positive corona discharges in air. *Journal of Physics D: Applied Physics*, *38*(13), 2211–2214. https://doi.org/10.1088/0022-3727/38/13/020

Parkevich, E. V., Shpakov, K. V., Baidin, I. S., Rodionov, A. A., Khirianova, A. I., Khirianov, T. F., et al. (2022). Streamer formation processes trigger intense X-ray and high-frequency radio emissions in a high-voltage discharge. *Physical Review E*, *105*(5), L053201. https://doi.org/10.1103/PhysRevE.105.L053201

Pasko, V. P. (2014). Electrostatic modeling of intra-cloud stepped leader electric fields and mechanisms of terrestrial gamma ray flashes. *Geophysical Research Letters*, *41*(1), 179–185. https://doi.org/10.1002/2013GL058983

Pasko, V. P., Janalizadeh, R., & Jansky, J. (2022). *Investigation of conditions necessary for inception of positive corona in air based on differential formulation of photoionization*. Abstract IF2.00005 presented at 75th Annual Gaseous Electronics Conference, Sendai, Japan, 3–7 October 2022.

Skeltved, A. B., Ostgaard, N., Carlson, B., Gjesteland, T., & Celestin, S. (2014). Modeling the relativistic runaway electron avalanche and the feedback mechanism with GEANT4. *Journal of Geophysical Research*, *119*(11), 9174–9191. https://doi.org/10.1002/2014JA020504

Stankevich, Y. L., & Kalinin, V. G. (1967). Fast electrons and X-ray radiation during the initial stage of growth of a pulsed spark discharge in air. *Soviet Physics, Doklady*, *12*, 1042–1043.

Stolzenburg, M., Marshall, T. C., Karunarathne, S., Karunarathna, N., Vickers, L. E., Warner, T. A., et al. (2013). Luminosity of initial breakdown in lightning. *Journal of Geophysical Research*, *118*(7), 2918–2937. https://doi.org/10.1002/jgrd.50276

Tilles, J. N., Krehbiel, P. R., Stanley, M. A., Rison, W., Liu, N., Lyu, F., et al. (2020). Radio interferometer observations of an energetic in-cloud pulse reveal large currents generated by relativistic discharges. *Journal of Geophysical Research*, *125*(20), e2020JD032603. https://doi.org/10.1029/2020JD032603

Zheleznyak, M. B., Mnatsakanyan, A. K., & Sizykh, S. V. (1982). Photoionization of nitrogen and oxygen mixtures by radiation from a gas discharge. *High Temperature*, *20*, 357–362.

Geophysical Research Letters
Supporting Information for

Conditions for inception of relativistic runaway discharges in air

Victor P. Pasko[1], Sebastien Celestin[2], Anne Bourdon[3], Reza Janalizadeh[1], and Jaroslav Jansky[4]

[1]School of Electrical Engineering and Computer Science, Penn State University, University Park, Pennsylvania, U.S.A.

[2]Laboratory of Physics and Chemistry of the Environment and Space (LPC2E), University of Orleans, CNRS, Orleans, France

[3]Plasma Physics Laboratory (LPP), Ecole Polytechnique, Palaiseau, France

[4]Department of Mathematics and Physics, University of Defense, Brno, Czechia

14 February 2023

Contents

List of Figures

1. Numerical implementation

1.1. Photoelectric effect in air

As expressed by equation (3) in the main text of the paper the number of runaway electrons produced per unit volume per unit time due to the photoelectric effect in air caused by air X-rays is given by:

$$S_{\rm pe}^{\rm air-X}(\vec{r}) = \int_{\varepsilon_{\rm run}(E_{\rm a})}^{\infty} \int_{V'} \xi_{\rm pe}\nu_\gamma(\varepsilon_\gamma) n_{\rm r}(\vec{r}\,') e^{-k_{\rm t}(\varepsilon_\gamma)R} \; \frac{n\sigma_{\rm pe}(\varepsilon_\gamma)}{4\pi R^2} dV' d\varepsilon_\gamma$$

The above expression can be written in the following form

$$S_{\rm pe}^{\rm air-X}(\vec{r}) = n \int_{V'} I(\vec{r}\,') \; \frac{g(pR, E_{\rm a})}{4\pi R^2} dV'$$

where p is air pressure, I=$\xi_{\rm pe}\nu_\gamma^{\rm t} n_{\rm r}$ and

$$\frac{g(pR, E_{\rm a})}{pR} = \frac{1}{pR} \int_{\varepsilon_{\rm run}(E_{\rm a})}^{\infty} \frac{\nu_\gamma(\varepsilon_\gamma)}{\nu_\gamma^{\rm t}} \; e^{-k_{\rm t}(\varepsilon_\gamma)R} \; \sigma_{\rm pe}(\varepsilon_\gamma) d\varepsilon_\gamma$$

Following *Bourdon et al.* [2007] and *Janalizadeh and Pasko* [2019] the integral form of $S_{\rm pe}^{\rm air-X}$ is replaced by an equivalent set of Helmholtz equations ($S_{\rm pe}^{\rm air-X} \propto n_{\rm r}$):

$$\nabla^2 S_{\rm pe}^i - (l_i \; p)^2 S_{\rm pe}^i = -p \; n \; C_i \; I$$

$$S_{\rm pe}^{\rm air-X} = \sum_i S_{\rm pe}^i$$

where the $l_{\rm i}$ and $C_{\rm i}$ are coefficients approximating $g(pR, E_{\rm a})/(pR)$ at a given applied electric field $E_{\rm a}$ using six exponential fits as described in [*Bourdon et al.*, 2007; *Janalizadeh and Pasko*, 2019]. Figure S1(b) illustrates propagator functions $g(pR, E_{\rm a})/(pR)$ for a selected values of applied electric field $E_{\rm a}$ covering range from $E_{\rm t}$ to $E_{\rm c}$. For practical calculations a dense array of $E_{\rm a}$ values is generated, each represented by six exponential fits. Due to smooth and continuous variation of the fit coefficients a simple linear interpolation is used to quickly find a coefficient set for any desired $E_{\rm a}$ value of the electric field during model execution.

1.2. Electrode effects

The photoelectric runaway electrons in air are produced due to X-rays emitted by anode upon bombardment by runaway electrons. We consider X-ray production from anode by choosing aluminum (Al) and tungsten (W) as two representative materials. The mean collisional stopping power of electrons in Al and W anodes considered in this work can be approximated as $\sim$2 MeV cm^2/g for the energy interval 100 keV to 10 MeV (https://physics.nist.gov/PhysRefData/Star/Text/ESTAR.html). A 100 keV electron in Al (mass density 2.7 g/cm^3) has stopping distance $l_{\rm s}$=0.2 mm. We use $l_{\rm s}$=2$\times$10^{-4} m value for all calculations presented in this work (it underestimates losses at lower energies and overestimates losses at higher energies).

We employ doubly differential cross-section of the bremsstrahlung photon production in Al and W following the same approach as for air. In comparison to air $\nu_\gamma^{\rm Al,W}(\varepsilon_\gamma)$ is enhanced by a factor of 10^3 for Al and 10^5 for W. The factor 10^3 comes from higher density $n_{\rm Al,W}$ of both materials, and the additional factor of 10^2 for W is due to Z^2 scaling of the the bremsstrahlung cross section with atomic number ($Z_{\rm N}$=7 and $Z_{\rm O}$=8 in air, and $Z_{\rm W}$=73).

We use direct integration to calculate contribution to production of runaway electrons in air due to X-rays emitted by anode:

$$S_{\rm pe}^{\rm anode-X}(\vec{r}) = \int_{\varepsilon_{\rm run}(E_{\rm a})}^{\infty} \int_{S'} \xi_{\rm pe} \nu_\gamma^{\rm Al,W}(\varepsilon_\gamma) n_{\rm r}(\vec{r}_{\rm A}) e^{-k_{\rm t}(\varepsilon_\gamma)R} \, \frac{n\sigma_{\rm pe}(\varepsilon_\gamma)}{4\pi R^2} l_{\rm s} dS' d\varepsilon_\gamma$$

where source integration is performed over anode surface S', $\vec{r}_{\rm A}$ denotes anode surface position vector, and R=$|\vec{r}-\vec{r}_{\rm A}|$. The total number of runaway electrons produced per unit volume per second in air due to the photoelectric absorption is then $S_{\rm pe}(\vec{r})$ = $S_{\rm pe}^{\rm air-X}(\vec{r}) + S_{\rm pe}^{\rm anode-X}(\vec{r})$.

The runaway electrons are emitted from the cathode due to the air and anode X-rays. Specifically, the X-rays produced by the bremsstrahlung radiation from air volume and the anode generate runaway electrons due to photoelectric absorption in the cathode:

$$S_{\rm pe}^{\rm air-X}(\vec{r}_{\rm C}) = \int_{\varepsilon_{\rm run}(E_{\rm a})}^{\infty} \int_{V'} \xi_{\rm pe} \nu_\gamma(\varepsilon_\gamma) n_{\rm r}(\vec{r}\,') e^{-k_{\rm t}(\varepsilon_\gamma)R} \, \frac{n_{\rm Al,W}\sigma_{\rm pe}^{\rm Al,W}(\varepsilon_\gamma)}{4\pi R^2} dV' d\varepsilon_\gamma$$

where R=$|\vec{r}_{\rm C}-\vec{r}\,'|$ is a distance between point of source $\vec{r}\,'$ and point of observation on cathode surface $\vec{r}_{\rm C}$, and similarly

$$S_{\rm pe}^{\rm anode-X}(\vec{r}_{\rm C}) = \int_{\varepsilon_{\rm run}(E_{\rm a})}^{\infty} \int_{S'} \xi_{\rm pe} \nu_\gamma^{\rm Al,W}(\varepsilon_\gamma) n_{\rm r}(\vec{r}_{\rm A}) e^{-k_{\rm t}(\varepsilon_\gamma)R} \, \frac{n_{\rm Al,W}\sigma_{\rm pe}^{\rm Al,W}(\varepsilon_\gamma)}{4\pi R^2} l_s dS' d\varepsilon_\gamma$$

where R=$|\vec{r}_{\rm C}-\vec{r}_{\rm A}|$ is a distance between points on the anode surface $\vec{r}_{\rm A}$ and point of observation on the cathode surface $\vec{r}_{\rm C}$, and in both cases $n_{\rm Al,W}$ and $\sigma_{\rm pe}^{\rm Al,W}(\varepsilon_\gamma)$ are number densities and photoelectric absorption cross sections, respectively, of cathode materials (illustrated by aluminum (Al) and tungsten (W) in this work). The total

runaway electron production rate due to the photoelectric absorption in the cathode material is $S_{\rm pe}(\vec{r}_{\rm C}) = S_{\rm pe}^{\rm air-X}(\vec{r}_{\rm C}) + S_{\rm pe}^{\rm anode-X}(\vec{r}_{\rm C})$.

Since in the energy region of interest in this work the propagation range of electrons is always shorter than the corresponding photon propagation distance, the electron stopping distance estimated above $l_{\rm s}$=2×10^{-4} m can be used as an effective cathode depth from which electrons can be released due to photoelectric absorption in cathode material. Having considered that the structure of $S_{\rm pe}(\vec{r}_{\rm C})$ integral is similar to the air integrals constituting $S_{\rm pe}(\vec{r})$, in practical calculations these effects are accounted for by multiplying the total $S_{\rm pe}(\vec{r})$ for air in the last cell of the simulation domain with size Δ by a ratio $(n_{\rm Al,W}\sigma_{\rm pe}^{\rm Al,W})/(n\sigma_{\rm pe})$, and by $l_{\rm s}/\Delta$, taking into account that emission of electrons occurs from volume with depth $l_{\rm s}$ near the cathode surface: $S_{\rm pe}(1) \rightarrow S_{\rm pe}(1) + S_{\rm pe}(1)\frac{n_{\rm Al,W}\sigma_{\rm pe}^{\rm Al,W}(\varepsilon_\gamma)}{n\sigma_{\rm pe}(\varepsilon_\gamma)}\frac{l_{\rm s}}{\Delta}$. This approximation is accurate only if the photoelectric absorption cross sections $\sigma_{\rm pe}^{\rm Al}$ and $\sigma_{\rm pe}^{\rm W}$ have the same dependence on energy ε_γ as $\sigma_{\rm pe}$ of air. This is a good approximation for Al with the corresponding cross section being a factor of 10 higher than that for air over a broad range of energies (https://www.nist.gov/pml/xcom-photon-cross-sections-database). The cross section for W has a complex structure with significant variations due to the K and L absorption edges, and the ratio varies between 10^3 at lower energies and 10^4 at energies 100 keV-1 MeV. In our calculations we approximate $(n_{\rm Al}\sigma_{\rm pe}^{\rm Al})/(n\sigma_{\rm pe})$ as 10^4, where factor of 10 comes from the ratio of cross sections and factor of 10^3 from the ratio of densities. We approximate $(n_{\rm W}\sigma_{\rm pe}^{\rm W})/(n\sigma_{\rm pe})$ as 10^7, where factor of 10^4 comes from the ratio of cross sections and factor of 10^3 from ratio of densities.

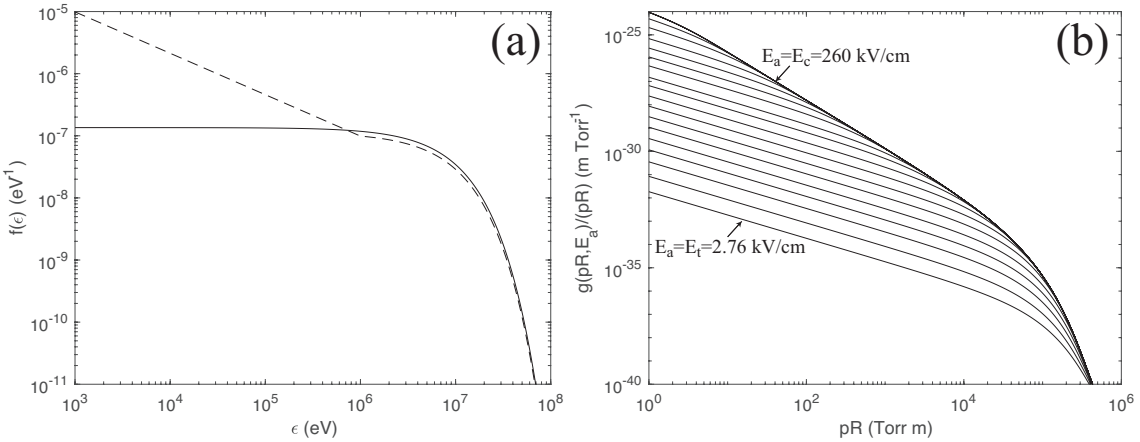

Figure S1: (a) The energy distribution function of relativistic runaway electrons used in all calculations in this work (solid line). Another model representation of this distribution containing a contribution from low energy secondary electrons is also shown for reference (dashed line) (see [*Dwyer et al.*, 2012, Figure 4 and references and discussion therein]). The model results are found to be essentially identical for both distributions. (b) Illustration of propagator functions $g(pR, E_{\rm a})/(pR)$ for a selected values of electric field $E_{\rm a}$ covering range from $E_{\rm t}$ to $E_{\rm c}$.

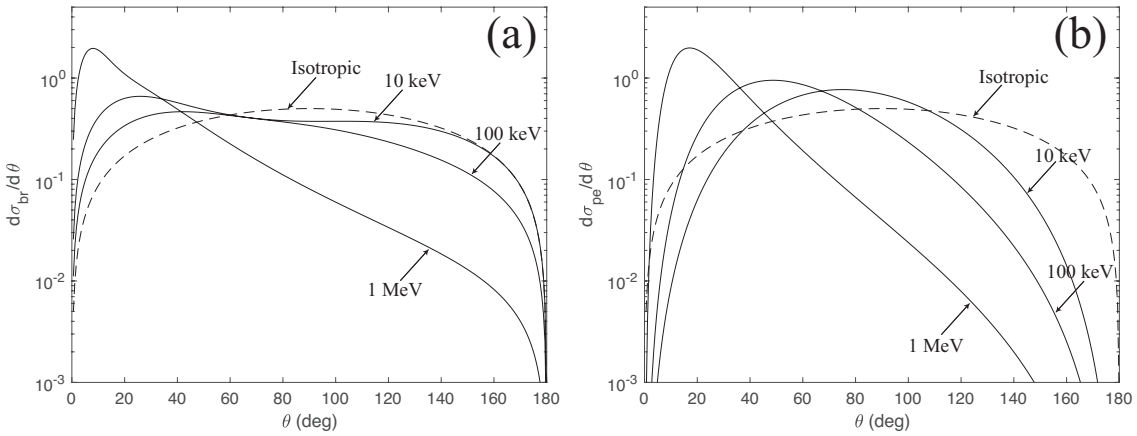

Figure S2: (a) The normalized to unity differential cross section ($\int_0^\pi \frac{d\sigma_{\rm br}}{d\theta} d\theta$=1) defining angular distribution of bremsstrahlung photons at selected photon energies [*Heitler*, 1954, p. 245]; [*Lehtinen*, March, 2000, p. 45, and references therein]. For reference the dashed line shows the isotropic distribution. (b) The normalized to unity differential cross section ($\int_0^\pi \frac{d\sigma_{\rm pe}}{d\theta} d\theta$=1) defining angular distribution of electrons produced by the photoelectric absorption at selected electron energies [*Carron*, 2007, p. 44]. For reference the dashed line shows the isotropic distribution.

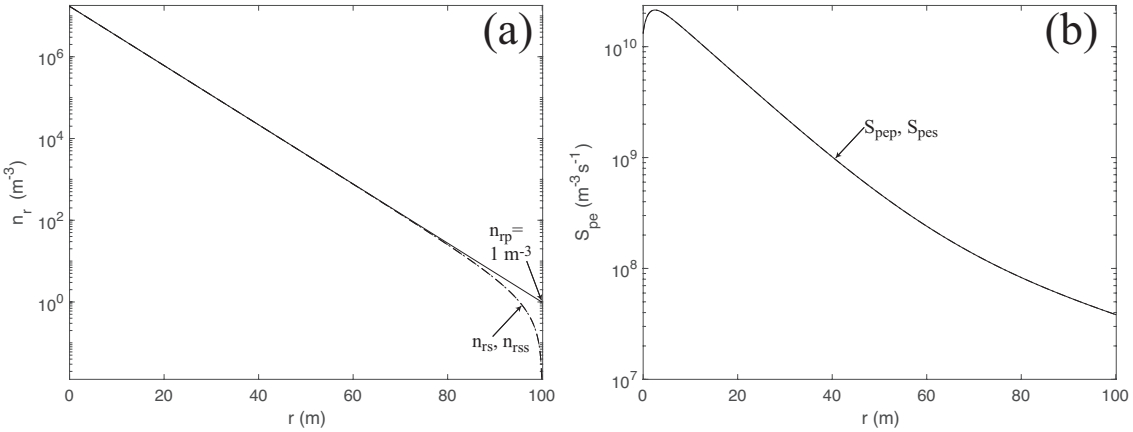

Figure S3: (a) The spatial distributions of runaway electrons $n_{\rm rs}$ and $n_{\rm rss}$ and the initial primary avalanche $n_{\rm rp}$ at the completion of the iteration process discussed in the text of main paper. The solution corresponds to $d\delta$=100 m, E_0/δ=1.51×10^6 V/m in Figure 3 taken at sea-level air pressure (δ=1). (b) The spatial distributions of the production rates of relativistic runaway electrons due to the photoelectric absorption, i.e., $S_{\rm pep}$ and $S_{\rm pes}$ corresponding to (a) (see main paper).

References

Bourdon, A., V. P. Pasko, N. Y. Liu, S. Célestin, P. Ségur, and E. Marode (2007), Efficient models for photoionization produced by non-thermal gas discharges in air based on radiative transfer and the Helmholtz equations, *Plasma Sources Sci. Technol.*, *16*(3), 656–678.

Carron, N. J. (2007), *An Introduction to the Passage of Energetic Particles through Matter*, Taylor and Francis, Boca Raton, FL.

Dwyer, J. R., D. M. Smith, and S. A. Cummer (2012), High-energy atmospheric physics: terrestrial gamma-ray flashes and related phenomena, *Space Sci. Rev.*, *173*(1-4), 133–196, doi:10.1007/s11214-012-9894-0.

Heitler, W. (1954), *The Quantum Theory of Radiation*, 3 ed., Clarendon, Oxford.

Janalizadeh, R., and V. P. Pasko (2019), A general framework for photoionization calculations applied to nonthermal gas discharges in air, *Plasma Sources Sci. Technol.*, *28*(10), 105006.

Lehtinen, N. G. (March, 2000), Relativistic runaway electrons above thunderstorms, Ph.D. dissertation, Stanford University, California.